SEMARAK ILMU PUBLISHING

Journal of Advanced Research in Fluid Mechanics and Thermal Sciences

Journal homepage:
https://semarakilmu.com.my/journals/index.php/fluid_mechanics_thermal_sciences/index
ISSN: 2289-7879

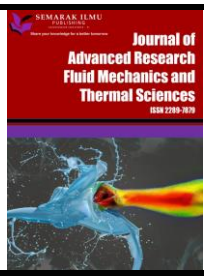

Airfoil Design and Aerodynamics Characteristics of Energy-Efficient Race Car: CFD Analysis

Barlin[1,2,*], Rido Firmansyah[1], Gunawan[1], Marwani[1], Astuti[1], Ellyanie[1]

[1] Department of Mechanical Engineering, Faculty of Engineering, Universitas Sriwijaya, 30139, Palembang, Indonesia
[2] Master Program of Material Science, Graduate School, Universitas Sriwijaya, 30139, Palembang, Indonesia

ARTICLE INFO

Article history:
Received 2 June 2024
Received in revised form 29 August 2024
Accepted 13 September 2024
Available online 30 September 2024

Keywords:
Aerodynamics; airfoil; Ansys fluent; Computational Fluid Dynamics (CFD); Taguchi method

ABSTRACT

The use of land transportation, primarily cars, is increasing annually. The energy required will increase along with the number of vehicles. Thus far, car manufacturers are required to improve car designs and propose fuel-efficient and environmentally friendly cars. The energy-efficient car competition, namely, Kontes Mobil Hemat Energi Indonesia, is organised for mechanical engineering students to contribute directly to research related to energy-efficient cars in Indonesia. One of the ways to save fuel is to reduce the aerodynamic force drag on the vehicle. This study aims to optimize the prototype vehicle airfoil design in producing the smallest possible coefficient of drag (Cd) and lift (Cl). A Taguchi design of experimental (DoE) is applied to set the 9 designs for this study, with three different values considered for each design parameters: Defiant Canard BL110, Clark YM15, Gottingen 256 for side airfoil shapes and Gottingen 410, Gottingen 460, and Boeing 737 Root for top airfoil shapes. This aerodynamic analysis uses the ANSYS 2020 R1 software, which is carried out at a speed of 30 km/h. Then the Cd and Cl values obtained will be analyzed. The results obtained for the optimal design of the Cd with variations in the side airfoil design Defiant Canard BL110 and top airfoil is Gottingen 410 with a Cd value of 0,1119. As for the optimal design of the Cl with variations in the side airfoil design Gottingen 256 and top airfoil is Gottingen 460 with a Cl value of 0,0250.

1. Introduction

The development of the transportation industry is improving worldwide, including in Indonesia. This improvement is consistent with Indonesia's population growth which continues to grow very rapidly in line with technological developments, and the need for energy is increasing. The main energy consumption of the transportation sector is energy fuel oil. The high use of fuel oil in the transportation sector is caused by the increasing number of motorized vehicles that use fuel oil, both public and private vehicles. The increase in energy demand, particularly oil and gas energy in Indonesia, can affect global warming, one of the problems that all countries face. Global warming is a condition where the ecosystem experiences imbalance due to increased land, sea and atmosphere

* *Corresponding author.*
E-mail address: barlin@ft.unsri.ac.id

https://doi.org/10.37934/arfmts.121.2.159173

temperatures. This increase occurs because of the burning of fossil fuels, namely, petroleum, in motorised vehicles. Reducing fuel consumption in vehicles is the right way to address fossil fuels as a non-renewable energy source and one of the causes of the greenhouse effect.

The existence of energy-efficient vehicles can undoubtedly affect the attempts to contain global warming. Saving fuel must be practised, considering that vehicles, primarily cars, still use fossil fuels. One of the ways to save energy is to reduce vehicle drag [1,2]. The smaller the drag value is, the less the fuel amount used is [3].

The previous researchers have explained that the competitions such as the Kontes Mobil Hemat Energi (KMHE) and the Shell Eco-Marathon are a forum for students to participate directly in research and create energy-efficient cars in the future [4-7]. Our study aims to find aerodynamic properties, the coefficients of drag and lift and the optimisation of the body with the design parameters of the side and top airfoil.

2. Methodology

This study used Computational Fluid Dynamics (CFD) with Ansys 2021 R1 software to obtain quantitative and qualitative data [8]. Quantitative data are in the form of coefficient of drag, drag force, coefficient of lift and lift force values, whereas the qualitative data are in the form of contour plots of static pressure distribution, velocity distribution, turbulence phenomena, flow streamlines and velocity vectors around the body. Making the prototype body design begins with selecting an airfoil for the initial body design. The prototype car body design uses two airfoil types: the upper body airfoil and the side body. In this study, three top and side airfoil variations produce nine prototype body variations. The prototype car body design intends to use two airfoil types. The nine designs refer to the side and top airfoil, as shown in Figure 1. On the side airfoil, only the front airfoil is used to provide space for the driver when driving a car. The top airfoil is used to design the top of the car. The combination of these two airfoil types reduces the friction coefficient and achieves an aerodynamic body.

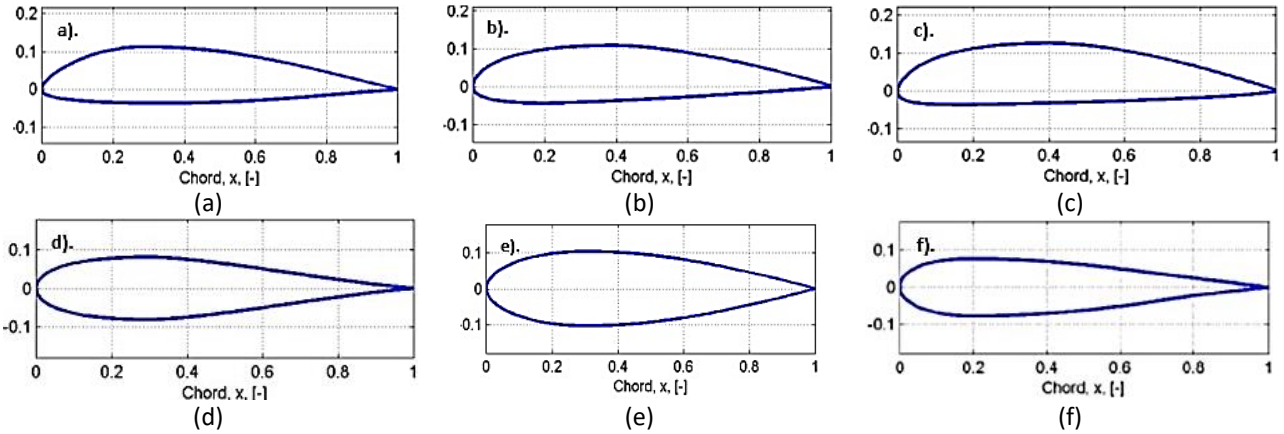

Fig. 1. Profile of side and top airfoil design (a) Defiant Canard BL110, (b) Clark YM15, (c) Gottingen 256, (d) Gottingen 410, (e) Gottingen 460, (f) Boeing 737 Root

The use of airfoil in vehicle design is determined using the Taguchi method. The Taguchi method proposes to obtain characteristic data using an orthogonal matrix and analyse the quality performance of the data to determine the optimal process parameters. The initial design in this study uses control variables (control factors), namely, the side airfoil profile and the top airfoil profile. Each variable uses three variations or levels. An orthogonal array matrix is used as an L^2 matrix (3^2). Based

on the variables and variations in Table 1, nine body designs can be made using the top and side airfoil profiles (Table 2). Table 3 shows the geometry properties of the side and top airfoil included in each design [9].

Table 1
Control factor and levels

Control Factors	Level		
	L1	L2	L3
Side airfoil profile	Defiant Canard BL110	Clark YM15	Gottingen 256
Top airfoil profile	Gottingen 410	Gottingen 460	Boeing 737 Root

Table 2
Matrix orthogonal array and distribution factor

Design No	Control Factors	
	Side airfoil profile	Top airfoil profile
1	Defiant Canard BL110	Gottingen 410
2	Defiant Canard BL110	Gottingen 460
3	Defiant Canard BL110	Boeing 737 Root
4	Gottingen 256	Gottingen 410
5	Gottingen 256	Gottingen 460
6	Gottingen 256	Boeing 737 Root
7	Clark YM15	Gottingen 410
8	Clark YM15	Gottingen 460
9	Clark YM15	Boeing 737 Root

Table 3
Geometry properties airfoil

Design No	Side airfoil geometry			Top airfoil geometry		
	Maximum Thickness	Boat-Tail Angle (deg)	Leading Edge	Maximum Thickness	Boat-Tail Angle (deg)	Leading Edge
1	14.7434% @0.3 C	16.2094	3.3505 %C	16.1%@0.3C	8.927	2.917 %C
2	14.7434% @0.3 C	16.2094	3.3505 %C	20.5 % @0.3C	27.4565	2.8239 %C
3	14.7434% @0.3 C	16.2094	3.3505 %C	15.3686% @0.3C	10.8793	3.4956 %C
4	14.8137% @0.33C	20.108	2.1275%C	16.1% @0.3C	8.927	2.917 %C
5	14.8137% @0.33 C	20.108	2.1275%C	20.5 % @0.3 C	27.4565	2.8239 %C
6	14.8137% @0.33 C	20.108	2.1275%C	15.3686% @0.3 C	10.8793	3.4956 %C
7	15.9444% @0.36 C	22.0788	4.3846%C	16.1% @0.3C	8.927	2.917 %C
8	15.944 % @0.36 C	22.0788	4.3846%C	20.5 % @0.3C	27.4565	2.8239 %C
9	15.9444 % @0.36 C	22.0788	4.3846%C	15.3686% @0.3C	10.8793	3.4956 %C

The considered prototype designs are shown in Figure 2. The designs are created using Ansys software. The frontal area is the area of the geometry exposed directly opposite the direction of the fluid. A vehicle design considering the frontal area can reduce aerodynamic drag. The area of the frontal area is obtained using SolidWorks software through the cavity menu. The size of this frontal area is included in the setup solution process in the reference value menu in the Ansys software (Figure 3).

Aerodynamic analysis is performed on nine designs with side and top airfoil variations at an air inlet speed of 30 km/h. The CFD simulation is conducted three times for each design to obtain the coefficient of drag and coefficient of lift. Then, the Cd and Cl values obtained are analysed using the Taguchi and Analysis of Variance (ANOVA) methods to determine the most optimal factors and levels in making body designs.

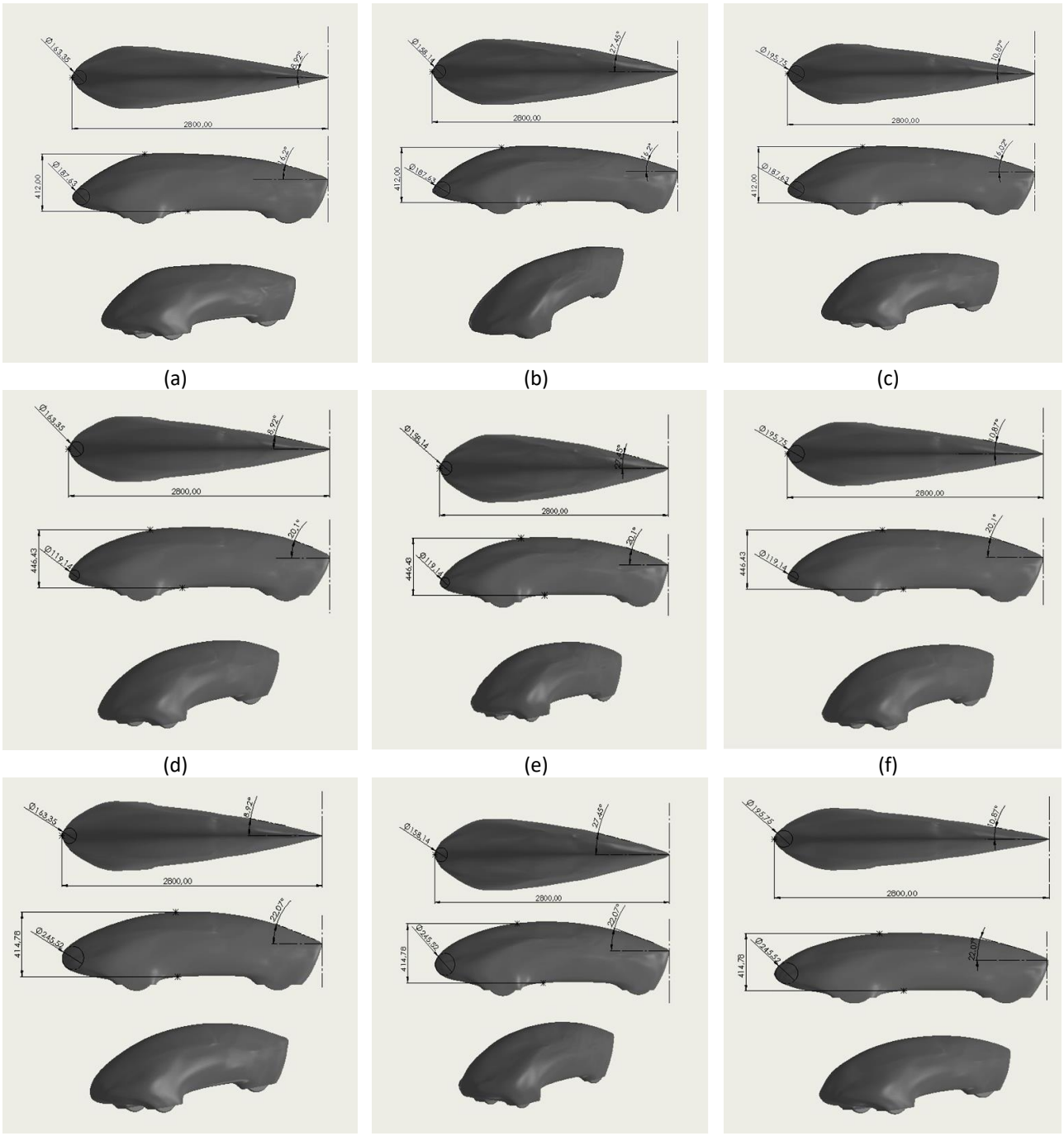

Fig. 2. Prototype car design (a) Design 1, (b) Design 2, (c) Design 3, (d) Design 4, (e) Design 5, (f) Design 6, (g) Design 7, (h) Design 8, (i) Design 9

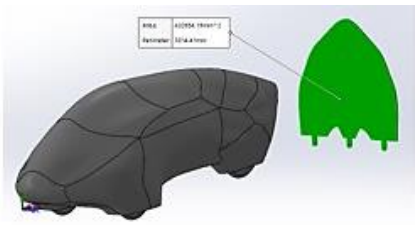

Design 1
Frontal area: 0,433 m^2

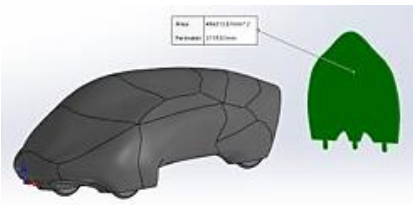

Design 2
Frontal area: 0,486 m^2

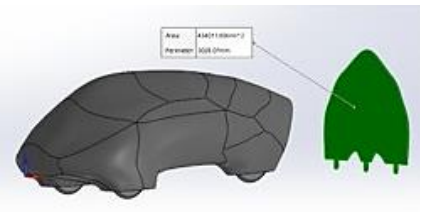

Design 3
Frontal area: 0,434 m^2

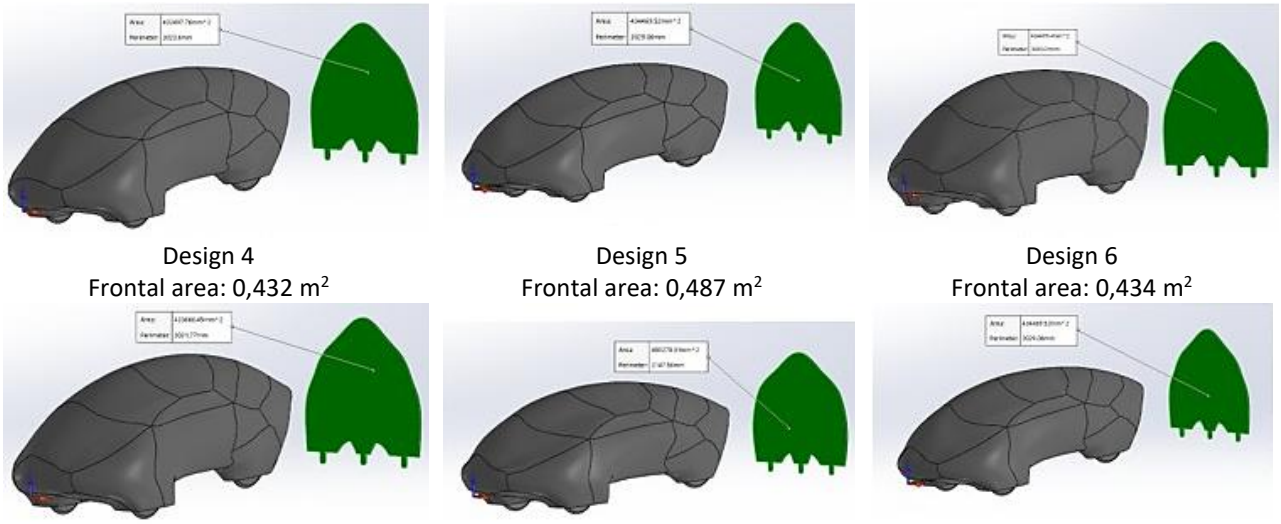

Design 4
Frontal area: 0,432 m^2

Design 5
Frontal area: 0,487 m^2

Design 6
Frontal area: 0,434 m^2

Design 7
Frontal area: 0,437 m^2

Design 8
Frontal area: 0,488 m^2

Design 9
Frontal area: 0,435 m^2

Fig. 3. Frontal area of each design

The enclosure manufacturing stage for the simulation domain is carried out in Geometry (Figure 4). The dimensions of the enclosure are length × width × height, for a length equal to seven times the length of the car. The width is equal to two times the length of the car, whereas the height is equal to two times the length of the car [10]. After the simulation domain is complete, the next step is naming the simulation domain, which is used as a constraint in the simulation (Figure 5). Nine simulation domain names are made: inlet, outlet, road, wall, front tire, rear tire, symmetry, a body of influence and vehicle body.

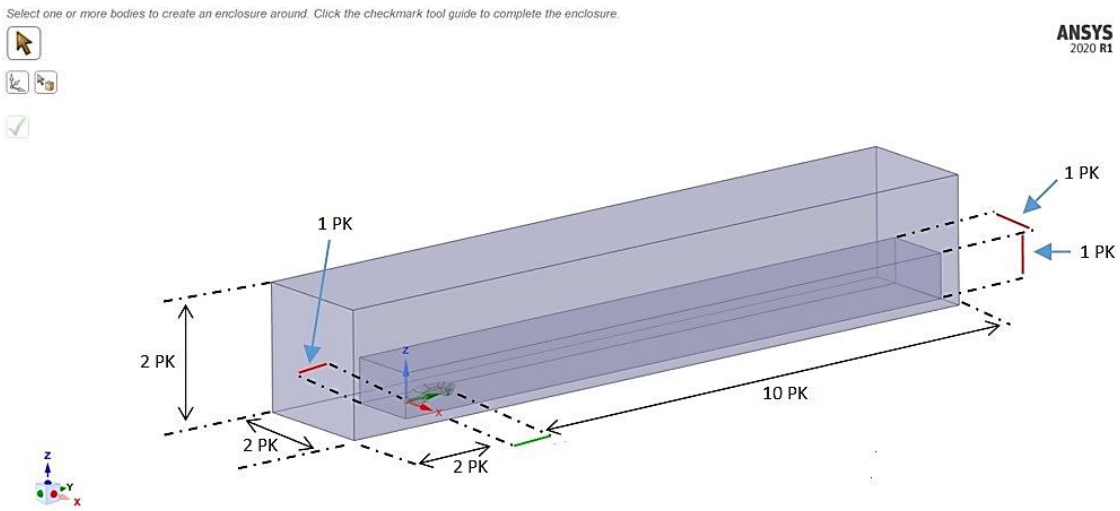

Fig. 4. Dimension domain simulation

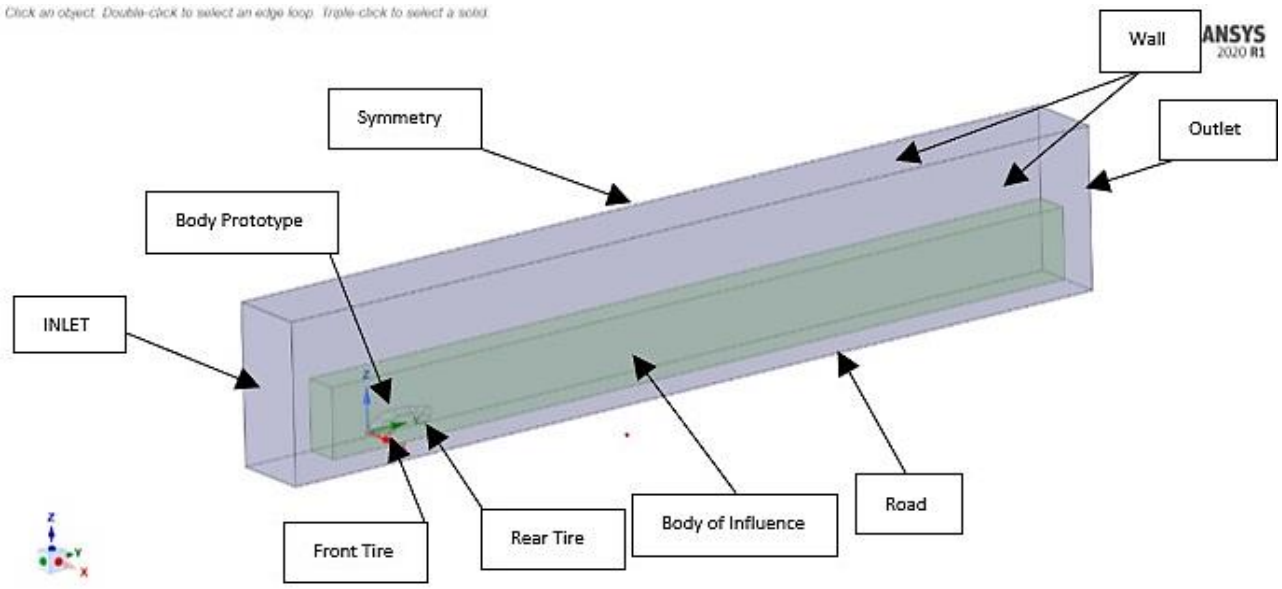

Fig. 5. Boundary condition

During meshing, a computational domain is divided into small parts, which control the volume. The geometry part undergoes a special treatment to mesh during the meshing stage are taken from the previous studies [6,11-14]. In the body of the influence mesh, the mesh size must be smaller than the simulation domain. In the prototype body, the mesh size must be smaller than the body of influence as shown in Table 4. Differences in mesh size in specific geometries are used to make the resulting contours in that area more detailed and make computer performance easier when performing simulations. The mesh quality considerably affects numerical computational accuracy and stability. Mesh size highly influences the computing speed and requirements. The smaller the mesh size is, the higher the number of formed cells is. Thus, a very heavy computation is required. When a surface mesh is created, the minimum surface mesh size is 0.01, whereas the maximum surface mesh size is 0.5 to obtain a mesh skewness value of less than 0.95 as shown in Table 5.

Table 4
Local sizing mesh

Local Sizing	Target Mesh Size
Body of Influence	0.1
Body Prototype	0.03

Table 5
Surface mesh size

Minimum size	Maximum size	Growth rate	Size functions	Curvature normal angle
0.03	0.5	1.2	Curvature	18

On the viscous model menu, the K-epsilon model is selected. This model is chosen because it can obtain a good boundary layer, and the pressure and velocity values to be analysed are considered [13]. The K-epsilon model is prevalent in industrial applications because of its reasonable convergence rate and relatively low memory requirements. The K-epsilon realisable model is chosen because it is most widely used in numerical simulations for prototype simulations. The nonequilibrium model is chosen because it explains the pressure gradient's effect on the velocity profile's distortion. The determination of boundary conditions can be seen in the Table 6. At a fluid velocity determined at 30 km/h, the inlet velocity is determined based on the KMHE 2022 Guideline.

In simulation, symmetry is one of the boundary condition parameters. The use of the symmetry section facilitates device performance in performing simulations. A wall boundary condition is applied for the vehicle body, road, front tire, rear tire and body of influence (Table 6).

Table 6
Boundary condition

Domain	Boundary condition	Unit
Inlet	Velocity Inlet	30 km/h
Outlet	Pressure Outlet	0 Pa
Road	Wall	No Slip
Front Tire	Wall	No Slip
Rear Tire	Wall	No Slip
Sym	Symmetry	-
Body Prototype	Wall	No Slip
Body of Influence	Wall	No Slip
Wall	Wall	Specified Shear

The fluid flow direction is calculated from the inlet in the reference values stage. The values of the vehicle length, the frontal area, and the velocity of the fluid are entered to find the value of the coefficients of drag and lift (Table 7). The solution method used in this analysis is the Semi-implicit Method for Pressure-linked Equations Consistent algorithm because it relates pressure and velocity.

Table 7
Reference value

Parameters	Value
Area (m^2)	0.432
Density (kg/m^3)	1.225
Enthalpy (j/kg)	0
Length (m)	2.8
Pressure (pascal)	0
Temperature (k)	288.16
Velocity (m/s)	13.0556
Viscosity (kg/m-s)	1.789e-05
Ratio of Specific Heat	1.4

3. Results

3.1 Simulation Results of Drag (CD) and Coefficient of Lift (*Cl)*

The simulated coefficients of drag and lift from the CFD analysis for nine designs are shown in Table 8 and Figure 6. The obtained data for the coefficients of drag and lift are analysed using statistical calculations known as ANOVA, which aims to determine the design parameters that significantly influence the quality characteristics of the body design [9]. ANOVA is processed by looking for two values that affect each contributing factor: ANOVA to the signal-to-noise ratio (SNR) and ANOVA to the mean value. A small value is used for the SNR. The smaller the obtained values of the coefficients of drag and lift are, the more optimal the produced design is.

Table 8
Simulation results of coefficient of drag dan lift for 9 designs

Design No	Side airfoil profile	Top airfoil profile	Coefficient of drag, Cd	Coefficient of lift, Cl
1	Defiant Canard BL110	Gottingen 410	0,10386	0,05806
2	Defiant Canard BL110	Gottingen 460	0,11143	0,03882
3	Defiant Canard BL110	Boeing 737 Root	0,10995	0,04548
4	Gottingen 256	Gottingen 410	0,12119	0,03735
5	Gottingen 256	Gottingen 460	0,11558	0,01411
6	Gottingen 256	Boeing 737 Root	0,11743	0,03041
7	Clark YM15	Gottingen 410	0,11075	0,03791
8	Clark YM15	Gottingen 460	0,11167	0,02216
9	Clark YM15	Boeing 737 Root	0,11032	0,0354

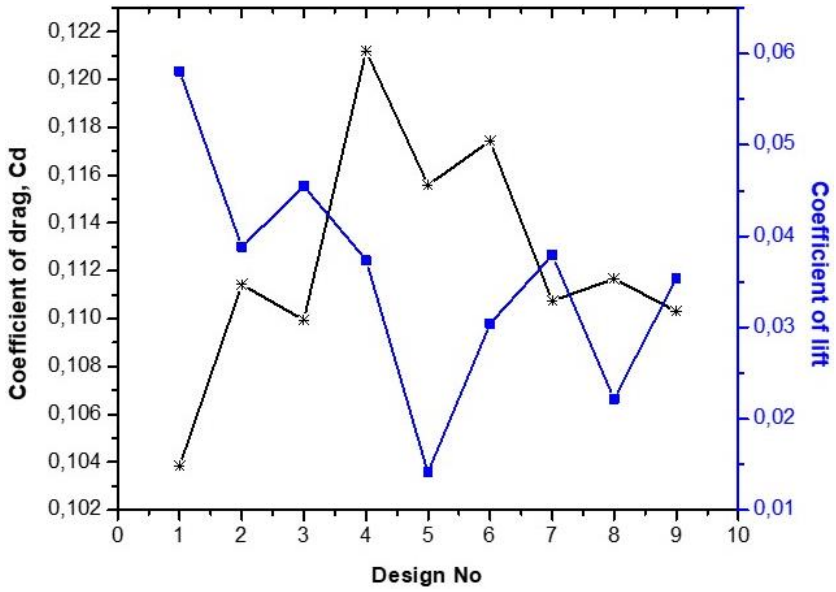

Fig. 6. Coefficient of drag and lift simulation result

In the Taguchi method, statistical calculations are performed to find factors influencing the mean response value. This statistical method is used to determine the most optimal level setting from the average response obtained from the previous studies [15-19]. After the average values for all car body designs are calculated, a response table and a response graph are made to compare the average response values in all experiments carried out on a factor. Then, the values are sorted from the largest to the smallest. Significant design parameters are identified using analysis of variance (ANOVA), and the optimal design is obtained using response tables and response graphs [20]. The coefficient of drag variance analysis is calculated based on the values from the response table. The data are obtained from ANOVA by comparing the F-ratio values to determine the factors with significant influence on the coefficients of drag and lift. The F-table estimates the distribution of F for the possible value, where (F0.05; N1 = 1; N2 = 18) the F-table is 4.41. The parameter is significant if the F-ratio value exceeds the F-table value [21]. Furthermore, the results of the data obtained are arranged as an ANOVA table.

The Anova results of the average Cd in Table 9 indicate that factor A (side airfoil design) has a smaller F-ratio value than the F-table. Thus, it does not significantly affect the coefficient of drag. For factor B (top airfoil design), the value of the F-ratio is greater than that of the F-table. Thus, factor B significantly influences the value of the coefficient of drag.

Table 9
ANOVA result for coefficient of drag

Source	SS	DF	MS	F Ratio	SS'	Ratio %	F Tabel	Effect
A	0,000474370	2	0,000237185	42,73102914	0,000463269	77%	3,44	insignificant
B	4,28566E-06	2	2,14283E-06	0,386049736	1,5387E-05	3%	3,44	significant
Error	0,000122114	22	0,000005551	1	0,000122114	20%		
SSt	0,000600770	26	0,000023107		0,00060077	100%		
Mean	0,34149845	1						
Sstotal	0,34209922	27						

A is side airfoil design and B is top airfoil design

For the average Cl in Table 10, factors A and B have a more considerable F-ratio value than the F-table. Factors A and B significantly influence the coefficient of lift. However, factor A has a significantly higher value than factor B, with a percentage contribution of 52% to the value of the coefficient of lift.

Table 10
ANOVA result for coefficient of lift

Source	SS	DF	MS	F Ratio	SS'	Ratio %	F Tabel	Effect
A	0,002014202	2	0,001007101	6,764957487	0,002002610	52%	3,44	significant
B	0,001728913	2	0,000864457	5,806776499	0,001717321	44%	3,44	significant
Error	0,000127512	22	0,000005796	1	0,000150696	4%		
SSt	0,003870628	26	0,000148870		0,003870628	100%		
Mean	0,034069333	1						
Sstotal	0,03793996	27						

A is side airfoil design and B is top airfoil design

3.2 Simulation Results of Contour Plots that Occur Around the Body
3.2.1 Static pressure distribution contour plots

Figure 7 shows the contour of static pressure distribution on the symmetry plane for each design variation. Red indicates high pressure, and green indicates low pressure. At the front of the body, the highest pressure occurs in the area with a stagnation point. The stagnation point occurs when the air moving in that area stops entirely at the front of the body, where the air velocity becomes zero and the highest static pressure occurs. In the middle of the body, the green contour means that the air velocity in that area is high enough to decrease the static pressure. The contour plot of each design shows the difference in colour and size. The larger the differences in colour and contour are, the greater the effect of static pressure on the pressure drag value is.

Figure 8 shows the contour plot of the static pressure on the surface of design body 1. Figure 8(a) shows a contour plot of the static pressure at the body's bottom. The lowest static pressure point occurs on the front fender of the front wheel, where the minimum static pressure value is −103.549. Figure 8(b) shows the static pressure contour plot at the top of the body. A stagnation point occurs on the front of the body where the moving air stops. Thus, the static pressure increases. The maximum pressure value that occurs in the body is 42.860 Pa.

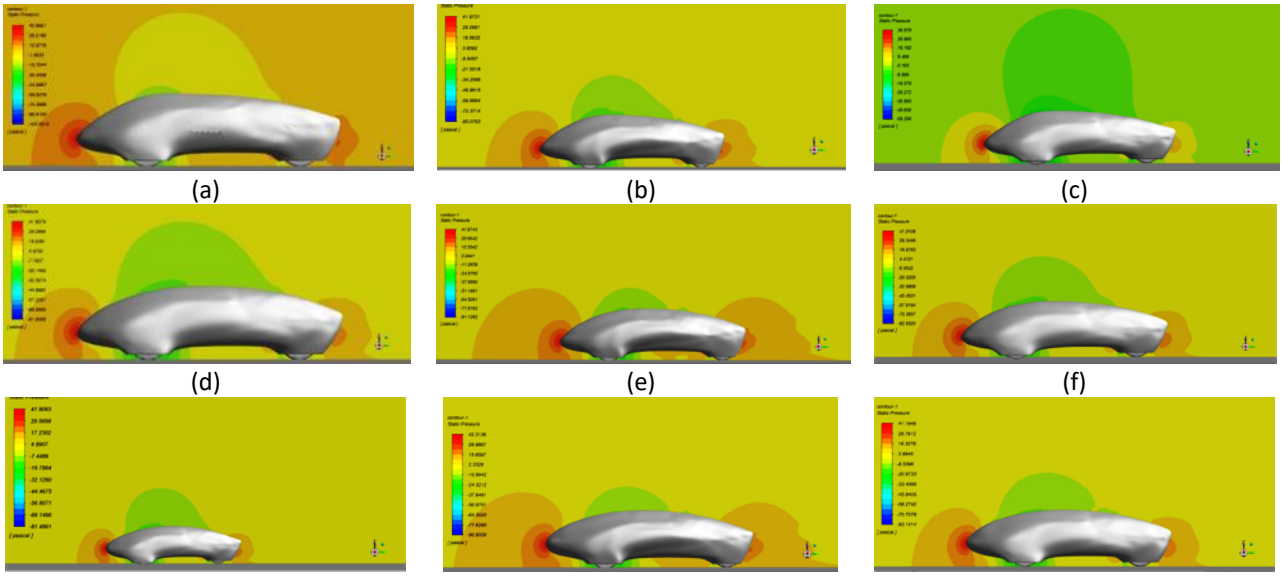

Fig. 7. Static pressure distribution at symmetry plane (a) Design 1, (b) Design 2, (c) Design 3, (d) Design 4, (e) Design 5, (f) Design 6, (g) Design 7, (h) Design 8, (i) Design 9

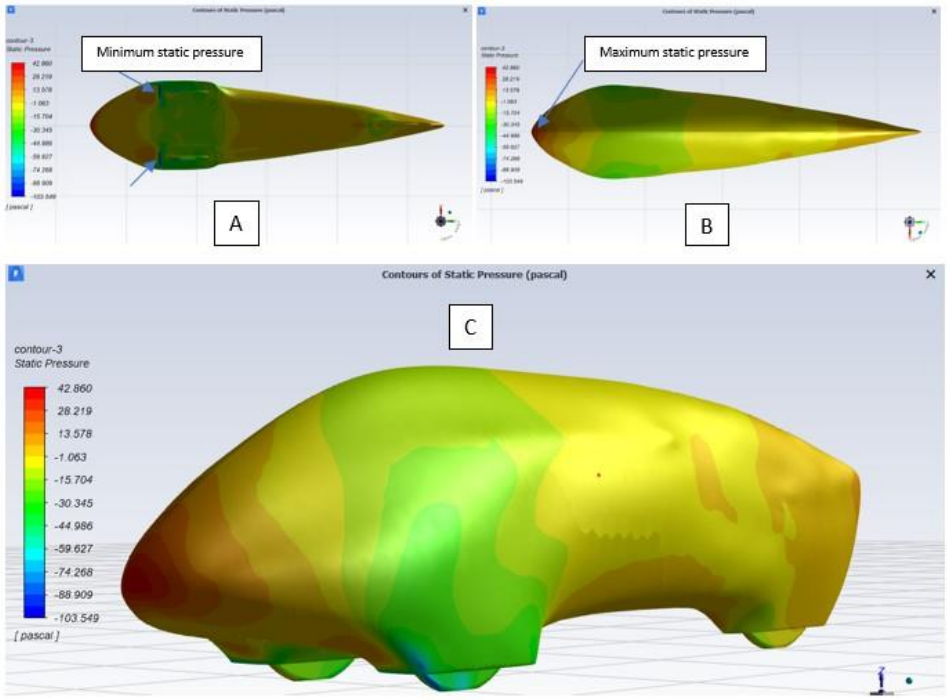

Fig. 8. Static pressure distribution on the body design 1

3.2.2 Air velocity contour plots

Figure 9 shows the contour plot of airspeed in the plane of symmetry for each design variation. The figure shows that low airspeed occurs on the front and rear of the body. At the back of the body is the area with the lowest airspeed, with a value of less than zero. In this area, wakes also occur, resulting in high drag. The highest airspeed occurs at the top of the car because of the high static pressure drop.

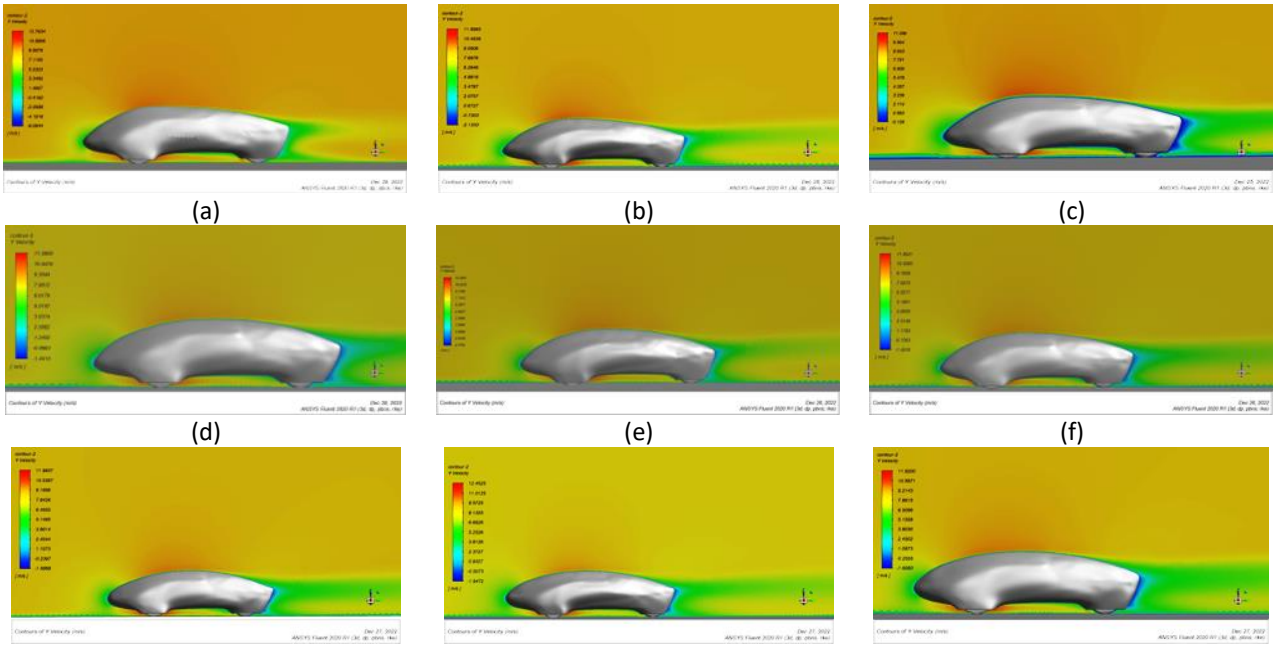

Fig. 9. Velocity distribution at symmetry plane (a) Design 1, (b) Design 2, (c) Design 3, (d) Design 4, (e) Design 5, (f) Design 6, (g) Design 7, (h) Design 8, (i) Design 9

Figure 10(a) shows that wakes occur on the front and rear fenders with the lowest airspeed value of −0.790 m/s. At the centre of the body and the centre of the front fender, the highest airspeed is 11.441 m/s. Wakes that occur because of low airspeed when passing vehicles affect the drag amount.

3.2.3 Turbulence phenomenon contour plots

Figure 10 shows the turbulence contour plot that occurs in the plane of symmetry. Turbulence occurs because of irregular airflow around the body. The difference in pressure and speed of the airflow passing through the lower and upper parts of the body causes irregular and twisting airflow when passing through the rear of the body. In each design, varying turbulence occurs. The drag force increases with the increase in wake contour and turbulence value generated. Amongst the other designs, design 1 has the lowest turbulence contours.

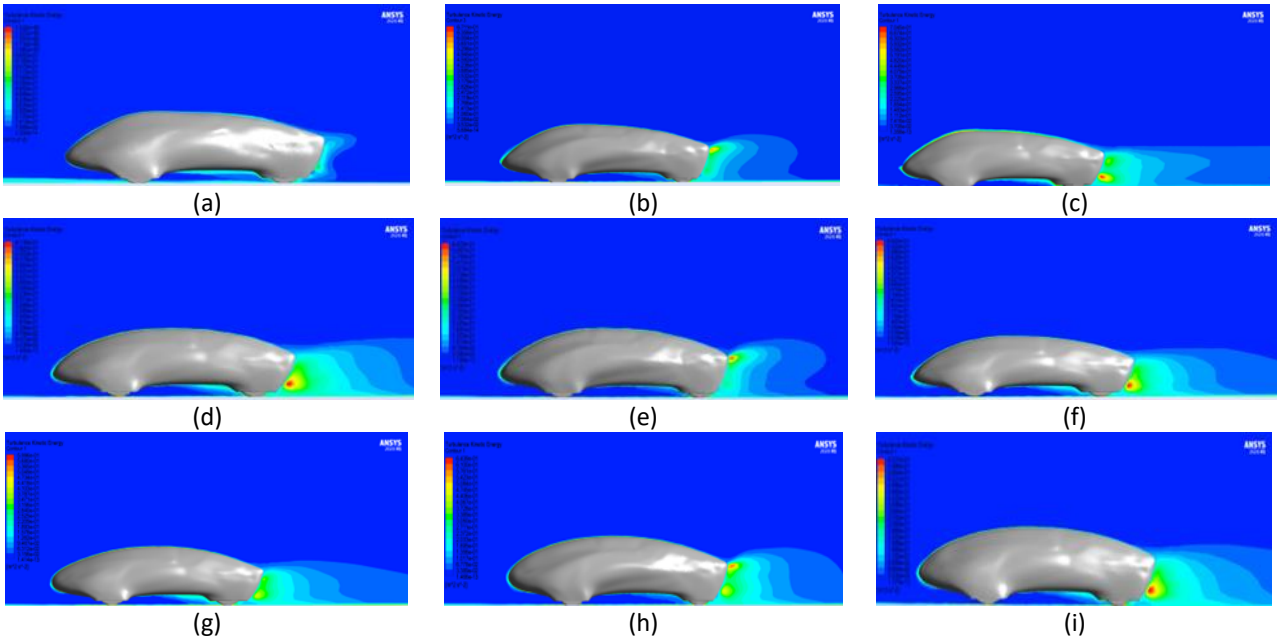

Fig. 10. Turbulence phenomenon contour plots at symmetry plane (a) Design 1, (b) Design 2, (c) Design 3, (d) Design 4, (e) Design 5, (f) Design 6, (g) Design 7, (h) Design 8, (i) Design 9

3.2.4 Streamline fluid flow

Figure 11 shows the streamlined contour plot of airflow on the plane of symmetry. The streamlined blue line at the back of the body indicates the flow velocity at 0 m/s. A rotating flow can cause wakes when the airflow passes through the back of the body. In the middle of the vehicle, the flow velocity increases from 9 m/s to 6 m/s, with the highest flow velocity observed between the front wheels.

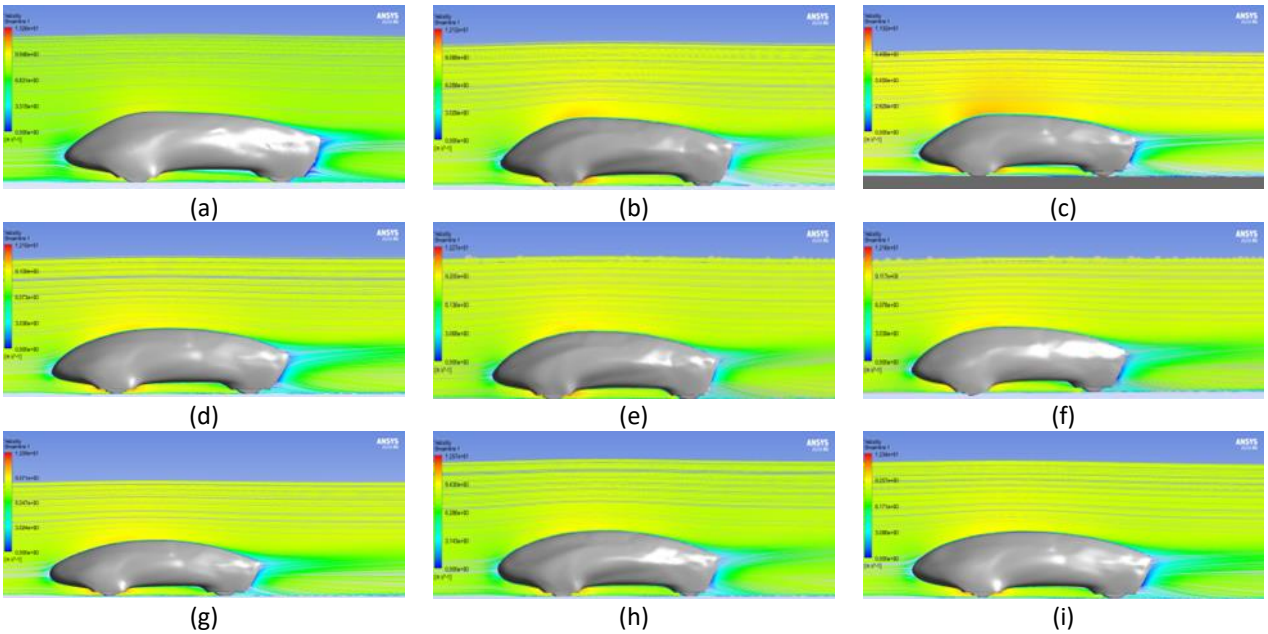

Fig. 11. Streamline fluid flow at symmetry plane (a) Design 1, (b) Design 2, (c) Design 3, (d) Design 4, (e) Design 5, (f) Design 6, (g) Design 7, (h) Design 8, (i) Design 9

3.2.5 Velocity vector around the body

Figure 12 shows the vector of air passing through the body. The velocity vector represents the stagnation point where the airflow stops, then turns and flows along the body's geometry. At the front of the body, the velocity vector is almost close to 0 m/s, while at the rear is the vector area with the lowest velocity. On the right and left sides of the body above the fender, the red and yellow speed vectors dominate, ranging from 8 m/s to 12 m/s. At the front of the front wheel fender is the vector with the highest speed because there is a significant drop in static pressure in that area.

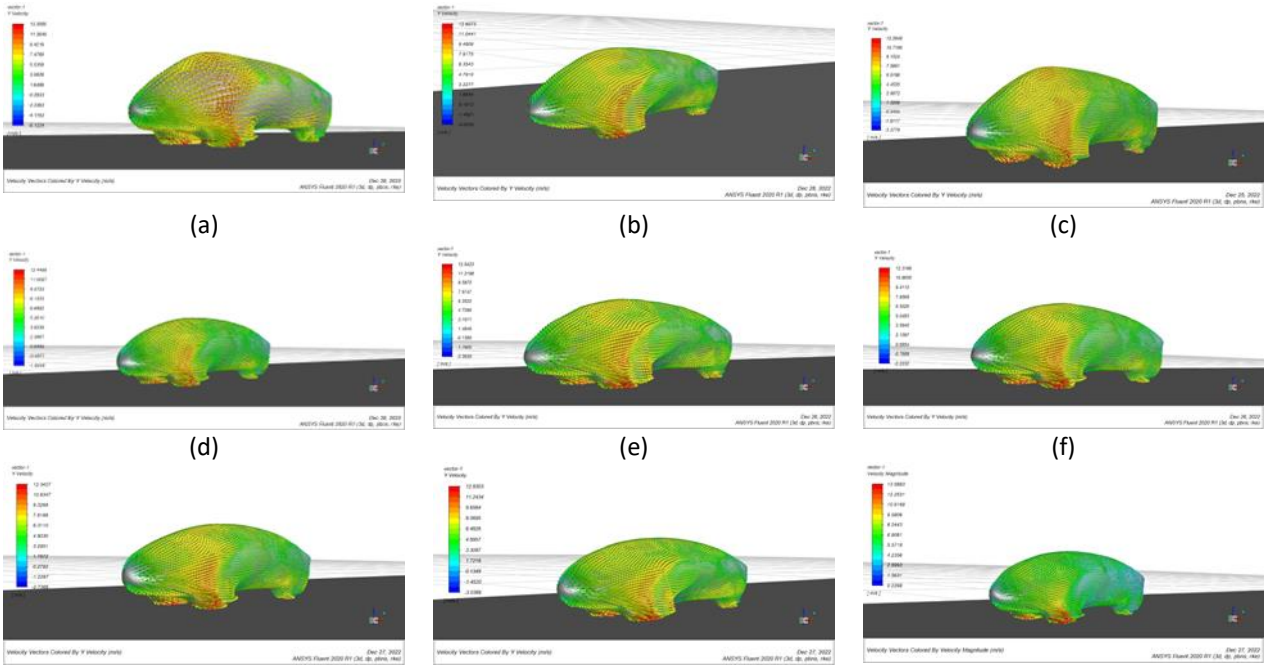

Fig. 12. Velocity vector around the body (a) Design 1, (b) Design 2, (c) Design 3, (d) Design 4, (e) Design 5, (f) Design 6, (g) Design 7, (h) Design 8, (i) Design 9,

The image of a velocity vector in the design symmetry field 1 is figured in Figure 13. On the front of the vehicle, the velocity vector is dominated by green and yellow colours, with the speed ranging from 3 m/s to 5 m/s. At the top of the body is the top speed vector of 10 m/s. A vector with negative velocity and rotating direction exists at the back of the body, causing wakes that increase drag.

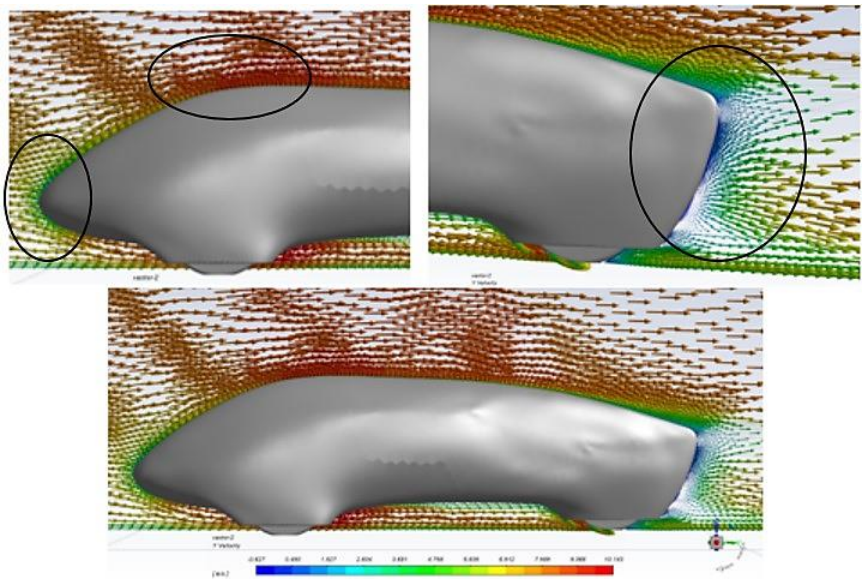

Fig. 13. Velocity vector design 1 at symmetry plane

4. Conclusions

In the coefficient of drag, the factor with a significant effect is factor B (top airfoil design) of the upper airfoil profile, with a percent contribution to the Cd of 73%. The optimum factor level for the upper airfoil profile is level 2: Gottingen 410 airfoil. Factor A has an insignificant effect, with a contribution percentage of 2% on the coefficient of drag. For the optimal factor level on factor A (side airfoil design), the side airfoil profile is the Defiant Canard BL110 Airfoil with an average coefficient of drag of 0.1119. The optimal level for factor B is Gottingen 410, with an average coefficient of drag of 0.1084. These results indicate that design 1 is the optimal design for obtaining a low coefficient of drag. On the coefficient of lift, all factors significantly influence the percentage contribution of factors A and B by 52% and 44%, respectively. The optimal level of factor side airfoil design is Gottingen 256 Airfoil with an average coefficient of lift of 0.0273. Moreover, the optimal level of factor top airfoil design is Gottingen 460 Airfoil, with an average coefficient of drag of 0.0250. These results indicate that design 5 is optimal in obtaining a low coefficient of lift.

Acknowledgment

The author would like to thank to the Universitas Sriwijaya for providing the facilities and equipment to support this research.

References

[1] Mansour, Hamdy, Rola Afify, and Omar Kassem. "Three-dimensional simulation of new car profile." *Fluids* 6, no. 1 (2020): 8. https://doi.org/10.3390/fluids6010008

[2] Vignesh, S., Vikas Shridhar Gangad, V. Jishnu, Amal Krishna, and Yagna S. Mukkamala. "Windscreen angle and Hood inclination optimization for drag reduction in cars." *Procedia Manufacturing* 30 (2019): 685-692. https://doi.org/10.1016/j.promfg.2019.02.062

[3] Marusic, Ivan, Dileep Chandran, Amirreza Rouhi, Matt K. Fu, David Wine, Brian Holloway, Daniel Chung, and Alexander J. Smits. "An energy-efficient pathway to turbulent drag reduction." *Nature Communications* 12, no. 1 (2021): 5805. https://doi.org/10.1038/s41467-021-26128-8

[4] Abidin, Harris Fadzillah Zainal, Md Tasyrif Abdul Rahman, Abdul Hamid Adom, Mohd Ridzuan Mohd Jamir, Sufi Suraya Halim, and Mohd Al Hafiz Mohd Nawi. "An Analysis of Urban Vehicle Body Aerodynamics Using Computational Fluid Dynamics for the Shell Eco-Marathon Challenge." *Journal of Advanced Research in Applied Sciences and Engineering Technology* 30, no. 2 (2023): 75-91. https://doi.org/10.37934/araset.30.2.7591

[5] Halim, Sufi Suraya, Md Tasyrif Abdul Rahman, Abdul Hamid Adom, Muhammad Sofwan Mohamad, Azizul Mohamad, and Nasrul Amri Mohd Amin. "Intake Manifold Material Selection and Fluid Flow Analysis for Formula Society of Automotive Engineers (FSAE) Race Car." *CFD Letters* 15, no. 5 (2023): 18-28. https://doi.org/10.37934/cfdl.15.5.1828

[6] Abo-Serie, Essam. "Aerodynamics assessment using CFD for a low drag Shell Eco-Marathon car." *Journal of Thermal Engineering* 3, no. 6 (2017): 1527-1536. https://doi.org/10.18186/journal-of-thermal-engineering.353657

[7] Nazaruddin, Nazaruddin, and Yudi Saputra. "Body Shape Selection of" Bono Kampar" For Urban Concept Student Car Formula to Fulfill Indonesian Energy-Saving Standards ("KMHE") with Aerodynamic Analysis." *CFD Letters* 12, no. 12 (2020): 104-114. https://doi.org/10.37934/cfdl.12.12.104114

[8] Oemar, Barlin, Zulkarnain Zulkarnain, Irsyadi Yani, Dendy Adanta, Amir Arifin, Gunawan Gunawan, Muhammad Abu Bakar Sidik, Ilham Saputra, Muhammad Wafiq Syadhefi, M. A. Ade Sapurta, and Ismail Thamrin. "Investigation of Effect Garbage Level in Filtration System to Headloss and Water Discharge by Computational Method." *CFD Letters* 14, no. 12 (2022): 99-110. https://doi.org/10.37934/cfdl.14.12.99110

[9] Melin, Tomas. "Parametric Airfoil Catalog Part I, Archer A18 to Göttingen 655: An Aerodynamic and Geometric Comparison Between Parametrized and Point Cloud Airfoils." *The Institute of Technology, Linköping University* (2013).

[10] Siregar, M. R., H. Kawai, and H. Ambarita. "Simulation on fuel consumption reduction of an urban concept car for energy-efficient competition." In *Journal of Physics: Conference Series*, vol. 1235, no. 1, p. 012096. IOP Publishing, 2019. https://doi.org/10.1088/1742-6596/1235/1/012096

[11] Yudianto, Aan, Herminarto Sofyan, Gunadi Gunadi, and Naufal Annas Fauzi. "Aerodynamic characteristics of overtaking bus under crosswind: CFD investigation." *CFD Letters* 14, no. 8 (2022): 20-32. https://doi.org/10.37934/cfdl.14.8.2032

[12] Zakher, Bassem Nashaat, Mostafa El-Hadary, Mohammed Abd Elfatah Elgohary, and Ibrahim M. El Fahham. "A Comparison Between Experimental Life Road Simulation and Computational Fluid Dynamics and Fluid Structure Interaction for Sedan Car." *CFD Letters* 14, no. 2 (2022): 81-97. https://doi.org/10.37934/cfdl.14.2.8197

[13] Fitriadhy, Ahmad, Intan Nur Nabila, Christina Bangi Grosnin, Faisal Mahmuddin, and Suandar Baso. "Computational Investigation into Prediction of Lift Force and Resistance of a Hydrofoil Ship." *CFD Letters* 14, no. 4 (2022): 51-66. https://doi.org/10.37934/cfdl.14.4.5166

[14] Arafat, Mohammad, Izuan Amin Ishak, Ahmad Faiz Mohammad, Amir Khalid, Md Norrizam Mohmad Jaát, and Mohd Fuad Yasak. "Effect of Reynolds number on the wake of a Next-Generation High-Speed Train using CFD analysis." *CFD Letters* 15, no. 1 (2023): 76-87. https://doi.org/10.37934/cfdl.15.1.7687

[15] Guharaja, S., A. Noorul Haq, and K. M. Karuppannan. "Optimization of green sand casting process parameters by using Taguchi's method." *The International Journal of Advanced Manufacturing Technology* 30 (2006): 1040-1048. https://doi.org/10.1007/s00170-005-0146-2

[16] Petuhov, Oleg. "Application of Taguchi optimization method in the preparation of activated carbon by microwave treatment." *Chemistry Journal of Moldova* 10, no. 1 (2015): 95-103. https://doi.org/10.19261/cjm.2015.10(1).14

[17] Kundu, Anirban, Bhaskar Sen Gupta, Mohd Ali Hashim, and Ghufran Redzwan. "Taguchi optimization approach for production of activated carbon from phosphoric acid impregnated palm kernel shell by microwave heating." *Journal of Cleaner Production* 105 (2015): 420-427. https://doi.org/10.1016/j.jclepro.2014.06.093

[18] Mia, Mozammel, and Nikhil Ranjan Dhar. "Optimization of surface roughness and cutting temperature in high-pressure coolant-assisted hard turning using Taguchi method." *The International Journal of Advanced Manufacturing Technology* 88 (2017): 739-753. https://doi.org/10.1007/s00170-016-8810-2

[19] Syed-Hassan, Syed Shatir Asghrar, and Mohd Saufi Md Zaini. "Optimization of the preparation of activated carbon from palm kernel shell for methane adsorption using Taguchi orthogonal array design." *Korean Journal of Chemical Engineering* 33 (2016): 2502-2512. https://doi.org/10.1007/s11814-016-0072-z

[20] Lee, Seungjun, Yohan Park, and Jin Kim. "An evaluation of factors influencing drag coefficient in double-deck tunnels by CFD simulations using factorial design method." *Journal of Wind Engineering and Industrial Aerodynamics* 180 (2018): 156-167. https://doi.org/10.1016/j.jweia.2018.07.018

[21] De Side, G. N., and N. N. Kencanawati. "An application of Taguchi experiment design methods on optimization of mortar mixture composition with Silica Fume as a partial substitute for cement." In *IOP Conference Series: Earth and Environmental Science*, vol. 413, no. 1, p. 012012. IOP Publishing, 2020. https://doi.org/10.1088/1755-1315/413/1/012012